Oral presentation | Multi-phase flow
Multi-phase flow-III
Mon. Jul 15, 2024 4:30 PM - 6:30 PM Room D

[3-D-03] Numerical study of dense particulate flows using Baer-Nunziato-like models

*Pavel Utkin[1] (1. Harbin Institute of Technology)

Keywords: Two-phase flow, Shock wave, Particle layer, Compressible flow, Compaction wave

Twelfth International Conference on Computational Fluid Dynamics (ICCFD12), Kobe, Japan, July 14-19, 2024

Numerical Study of Dense Particulate Flows using Baer-Nunziato-like Models

P. Utkin*
Corresponding author: utkin@hit.edu.cn
* Department of Astronautical Science and Mechanics,
Harbin Institute of Technology, China

Abstract: This work focuses on the study of the mechanisms behind the amplification of disturbances propagating through a dense sand bed under repeated impact of a normal shock wave, a phenomenon recently discovered in experiments. The Baer-Nunziato model and the Godunov numerical method were employed. The model and method were verified by solving problems such as normal incidence of a shock wave on a particle curtain, normal incidence of a shock on a layer of particles close to the wall, and propagation of a shock along a particle layer. It was found that wave amplification can be attributed to intergranular stress effects in the particle phase, but the model still requires further refinement to ensure attenuation of disturbances as they propagate deeper into the bed.

Keywords: Two-phase flows, compressible flows, shock wave, intergranular stresses, compaction wave, particle layer, Godunov method.

1 Introduction

Simulations of high-speed compressible flows with shock waves in the presence of dense layers of particles, with a significant volume fraction of the solid phase, are relevant in various fields. These simulations arise in problems related to explosion safety, such as the dispersion of particles behind a shock wave during a dust explosion [1], as well as in the development of explosion-proof coatings [2]. They are also relevant in fire extinguishing systems, where shock-induced gas-particle jets play a significant role [3]. Additionally, they are important in energetics, specifically the propagation of combustion waves in localized charges of heterogeneous explosives [4]. Military technologies such as explosive dispersion of solid particles into the surrounding air [5] and penetration of high-speed bodies through a granular medium are also dependent on these simulations [6]. Furthermore, the oil-and-gas industry [7], aerospace research, such as interactions between rocket exhaust plumes and the surface of extraterrestrial bodies during spacecraft landings [8], and other fields, all rely on these simulations for their research and development. Although many of these issues have been studied for years, mathematical models and computational techniques for simulating high-speed flows of dense two-phase media were developed more recently and are still being actively developed. Baer-Nunziato-type models [9] are commonly used to simulate the deflagration-to-detonation transition in heterogeneous explosives and two-phase flows containing droplets or bubbles. However, these models are not often used to model two-phase flows where the compressibility of the dispersed phase is much less than that of the continuous phase, see [10] as an example. Although compressible models can be more computationally intensive, they offer a different perspective on the wave process within a layer of particles compared to models based on kinetic theory for granular media [11 – 14] or models of a gas-saturated porous medium with two stress tensors [15 – 17], and some variations [18]. In these models, particles are considered incompressible.

In a series of previous papers, we have considered various problems related to dense particulate flows using Baer-Nunziato-like models. Specifically, in [19 – 21], we examined the interaction between a shock wave and a particle bed (the Rogue shock tube test [22]), see Figure 1. This problem has been studied in many papers using various two-phase models as a case study, see the review in [20]. The overall mechanisms of this process are well understood, but the specific details, such as reflected and transmitted waves and moving interface boundaries, still need further investigation in simulations, see [23]. Clearly, this case study remains a challenging problem for new two-phase flow models. The paper [24] shows an example of not very good simulation results for the Rogue shock tube experiment.

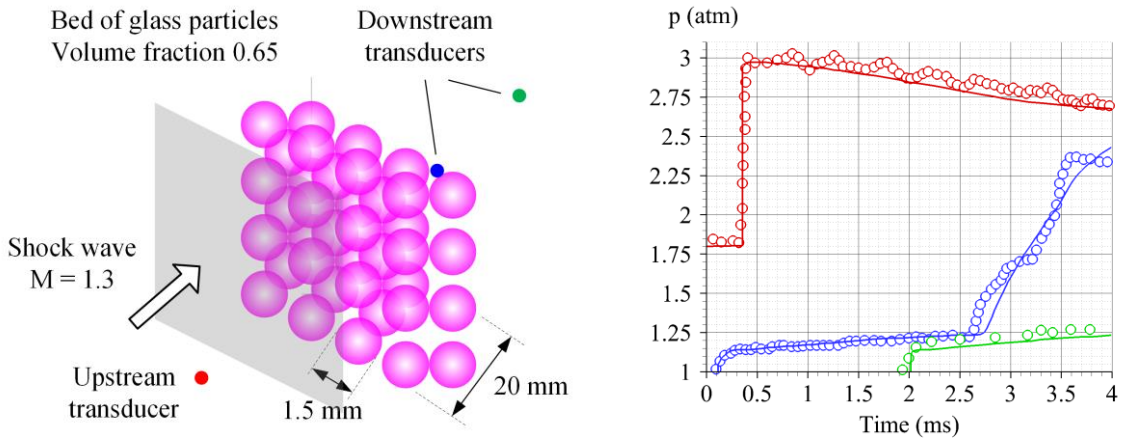

(a) (b)

Figure 1: A test of a shock wave interacting with a bed of particles: (a) a schematic of the setup [22], (b) a comparison of computed pressure measurements (lines) [21] with experimental data (dots).

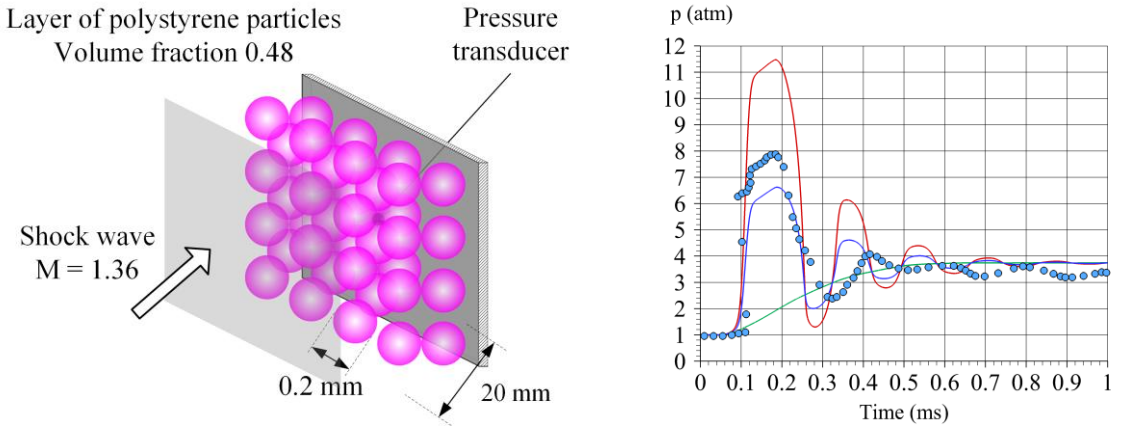

(a) (b)

Figure 2: A test with a normally incident shock wave interacting with a layer of particles on a surface: (a) the schematic of the problem [25], (b) the comparison of the computed record of a pressure transducer on the surface under the layer of particles [21]. The lines represent the solid phase pressure (red), the gaseous phase pressure (green), and the volume averaged pressure (blue), while the dots represent the experimental data.

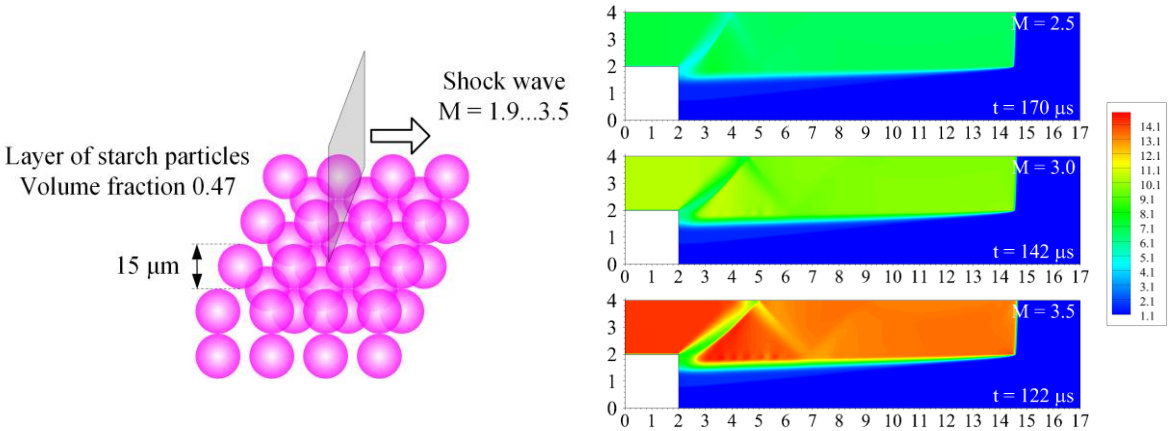

(a) (b)

Figure 3: Test with a shock wave propagating over a layer of particles: (a) the schematic of the setup [28], (b) predicted gas pressure distributions for various intensities of the shock wave [27]. Axes are in centimeters and the pressure scale is in atmospheres.

In [21], we explored the effect of pressure rise under a layer of particles due to the impact of a normally incident shock wave (see Figure 2). The model takes into account both reversible and irreversible compaction of the layer. For the simulation, we used the Godunov method for the Baer-Nunziato equations [26]. Our recent paper [27] is about the simulation of the propagation of a shock wave over a layer of particles (see Figure 3). The setup of the problem corresponds to the experiment [28]. We obtained the correct dependence of the granular contact angle and transmitted compaction angle on the intensity of the shock wave, similar to the experiment, and we explained it.

The aim of this study is to investigate the possible mechanisms behind the effect of shock wave amplification in the dense sand layer, which was recently observed in experiments [29, 30], using the Baer-Nunziato model.

2 Problem Statement

The statement follows the experiments conducted by [29] and [30]. These experiments were carried out using a conventional shock tube facility that was equipped with a section containing a granular medium (see Figure 4). The parameters in the high-pressure chamber were as follows:

$$\rho_{\mathrm{HPC}} = 1.63\ \mathrm{kg/m^3}, p_{\mathrm{HPC}} = 1.37\ \mathrm{atm}, T_{\mathrm{HPC}} = 293\ \mathrm{K}, u_{\mathrm{HPC}} = 0\ \mathrm{m/s}.$$

All notations used are standard. The parameters in the low-pressure chamber were:

$$\rho_{\mathrm{LPC}} = 1.19\ \mathrm{kg/m^3}, p_{\mathrm{LPC}} = 1.0\ \mathrm{atm}, T_{\mathrm{LPC}} = 293\ \mathrm{K}, u_{\mathrm{LPC}} = 0\ \mathrm{m/s}.$$

Air was used as the working gas. Initial shock wave Mach number was about 1.08. To measure the pressure, four pressure records D1 – D4 were used. The granular medium used was dry sand with an average particle diameter of $d = 390$ micrometers. The true density of the sand was assumed to be $\bar{\rho}_0 = 2620\ \mathrm{kg/m^3}$.The initial volume fraction of particles was $\bar{\alpha}_0 = 0.65$.

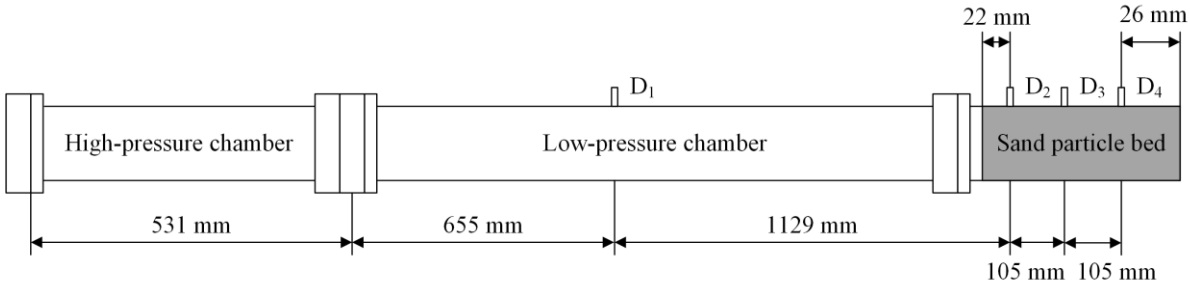

Figure 4: A schematic of the experimental setup.

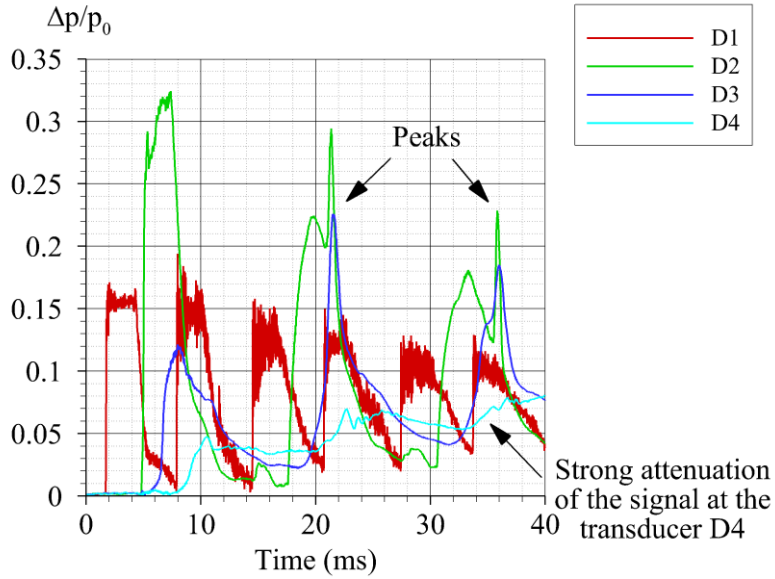

Figure 5: Recordings of pressure transducers during the experiment [30].

Experimental relative pressure increments $\Delta p/p_0 = (p - p_0)/p_0$ for four pressure transducers are shown in Figure 5. One of the main experimental observations from [29, 30] is that transducers D2 and D3, located inside the particle bed, measure pressure peaks, while transducer D4 shows strong attenuation of the signal. This is in contrast to the previous papers [2, 16, 17, 21, 25], which found that disturbances in a two-phase medium were amplified on the wall under the bed, rather than inside the bed. The current work aims to explore possible mechanisms behind this effect.

3 Numerical Setup

The mathematical model is based on the Baer-Nunziato equations [9] with the subsequent modifications made by [31, 32] regarding compaction terms. The defining system of equations has the following form [33]:

$$\mathbf{u}_t + \mathbf{f}_x(\mathbf{u}) = \mathbf{h}(\mathbf{u})\bar{\alpha}_x + \mathbf{p} + \mathbf{s},$$

$$\mathbf{u} = \begin{bmatrix} \bar{\alpha} \\ \bar{\alpha}\bar{\rho} \\ \bar{\alpha}\bar{\rho}\bar{u} \\ \bar{\alpha}\bar{\rho}\bar{E} \\ \alpha\rho \\ \alpha\rho u \\ \alpha\rho E \end{bmatrix}, \quad \mathbf{f} = \begin{bmatrix} 0 \\ \bar{\alpha}\bar{\rho}\bar{u} \\ \bar{\alpha}(\bar{\rho}\bar{u}^2 + \bar{p}) \\ \bar{\alpha}\bar{u}(\bar{\rho}\bar{E} + \bar{p}) \\ \alpha\rho u \\ \alpha(\rho u^2 + p) \\ \alpha u(\rho E + p) \end{bmatrix}, \quad \mathbf{h} = \begin{bmatrix} -\tilde{u} \\ 0 \\ \tilde{p} \\ \tilde{p}\tilde{u} \\ 0 \\ -\tilde{p} \\ -\tilde{p}\tilde{u} \end{bmatrix}, \quad \mathbf{p} = \begin{bmatrix} F \\ 0 \\ 0 \\ -\tilde{p}F \\ 0 \\ 0 \\ \tilde{p}F \end{bmatrix}, \quad \mathbf{s} = \begin{bmatrix} 0 \\ 0 \\ M \\ I \\ 0 \\ -M \\ -I \end{bmatrix},$$

$$\alpha + \bar{\alpha} = 1,$$

$$\bar{E} = \frac{\bar{u}^2}{2} + \frac{\bar{p} + \bar{\gamma}\bar{P}_0}{\bar{\rho}(\bar{\gamma} - 1)} + B(\bar{\alpha}), \quad E = \frac{u^2}{2} + \frac{p}{\rho(\gamma - 1)},$$

$$F = \frac{\alpha\bar{\alpha}}{\mu_c}(\bar{p} - \tilde{p} - \beta), \quad \beta = \bar{\alpha}\bar{\rho}\frac{dB}{d\bar{\alpha}}.$$

Here α is the volume fraction, u is the velocity, ρ is the density, p is the pressure, E is the total specific energy, $\bar{\gamma}$ and $\bar{P}_0$ are the constant parameters in the stiffened gas equations of state for the dispersed phase, γ is the specific heat ratio of the gas, μ_c is the coefficient of compaction viscosity, $\beta(\bar{\alpha}, \bar{\rho})$ is an intergranular stress. The bar superscript indicates dispersed phase variables throughout the paper.

Velocity $\tilde{u}$ and pressure $\tilde{p}$ are interfacial variables. These are chosen as follows [9]:

$$\tilde{p} = p, \quad \tilde{u} = \bar{u}.$$

For the problem under consideration, the following parameters are used in the equations of state of the phases:

$$\bar{\gamma} = 2.5, \quad \bar{P}_0 = 10^7 \text{ Pa}, \quad \gamma = 1.4.$$

The vector **p** contains terms related to pressure relaxation. In the current work, we take into account the following condition of mechanical equilibrium at the interface boundary [34]:

$$\bar{p} = \tilde{p} + \beta,$$

$$\beta = \bar{\alpha}\bar{\rho}\frac{dB}{d\bar{\alpha}} = -\bar{\alpha} \cdot \bar{\rho} \cdot a \cdot n \cdot \ln\frac{1 - \bar{\alpha}}{1 - \bar{\alpha}_{\text{crit}}} \cdot \left(\frac{B(\bar{\alpha})}{a}\right)^{\frac{n-1}{n}},$$

$$B(\bar{\alpha}) = \begin{cases} B_a(\bar{\alpha}), & \text{if } \bar{\alpha}_{\text{crit}} < \bar{\alpha} < 1.0, \\ 0, & \text{otherwise}, \end{cases} \tag{1}$$

$$B_a(\bar{\alpha}) = a \cdot [b_1(\bar{\alpha}) - b_1(\bar{\alpha}_{\text{crit}}) + b_2(\bar{\alpha})]^n,$$

$$b_1(\bar{\alpha}) = (1-\bar{\alpha})\cdot\log(1-\bar{\alpha}), \quad b_2(\bar{\alpha}) = \left(1+\log(1-\bar{\alpha}_{\text{crit}})\right)\cdot(\bar{\alpha}-\bar{\alpha}_{\text{crit}}).$$

Here, $B(\bar{\alpha})$ is the potential energy of compaction, a and n are the parameters of the compaction law that are characteristics of the material, $\bar{\alpha}_{\text{crit}}$ is the volume fraction of the dispersed phase when compaction begins and $B(\bar{\alpha})$ becomes nonzero. The values of the parameters used in the compaction law are:

$$a = 2.5\cdot 10^3 \text{ J/kg}, \quad n = 1.02, \quad \bar{\alpha}_{\text{crit}} = 0.66.$$

The vector **s** contains source terms that describes the exchange of mass, momentum, and energy between the different phases. The *M* term describes the interfacial momentum exchange while the *I* term describes interfacial energy exchange. Correlations from [11, 13] were used to describe the interphase interaction:

$$M = -K(\bar{u}-u), \quad I = -M\tilde{u},$$

$$\text{Re} = \frac{\rho|\bar{u}-u|d}{\mu_{\text{vis}}},$$

$$K = \begin{cases} 0.75C_D\dfrac{\rho\bar{\alpha}|\bar{u}-u|}{d\alpha^{1.65}}, & \text{if } \alpha \geq 0.8, \\ \dfrac{150\bar{\alpha}^2\mu_{\text{vis}}}{\alpha d^2} + 1.75\dfrac{\rho\bar{\alpha}|\bar{u}-u|}{d}, & \text{if } \alpha < 0.8, \end{cases}$$

$$C_D = \begin{cases} \dfrac{24}{\alpha\text{Re}}[1+0.15(\alpha\text{Re})^{0.687}], & \text{if } \alpha\text{Re} < 10^3, \\ 0.44, & \text{if } \alpha\text{Re} \geq 10^3. \end{cases}$$

Here d is the particle's diameter and μ_{vis} is the dynamic gas viscosity coefficient.

The computational algorithm is based on the Strang splitting principle. At each time step, a hyperbolic sub-step (the first stage of the algorithm) is performed, followed by a pressure relaxation sub-step (the second stage), and then non-differential algebraic source terms describing interfacial interaction (the third stage) are taken into account. The hyperbolic step is performed using the Godunov method [26]:

$$\mathbf{U}_i^{h,n+1} = \mathbf{U}_i^n - \frac{\Delta t^n}{\Delta x}[\mathbf{F}_{\text{L}}(\mathbf{U}_i^n, \mathbf{U}_{i+1}^n) - \mathbf{F}_{\text{R}}(\mathbf{U}_{i-1}^n, \mathbf{U}_i^n)],$$

$$\mathbf{F}_{\text{L}}(\mathbf{U}_i^n, \mathbf{U}_{i+1}^n) = \begin{cases} \mathbf{f}[\mathbf{U}^*(\mathbf{U}_i^n, \mathbf{U}_{i+1}^n)] - \mathbf{H}(\mathbf{U}_i^n, \mathbf{U}_{i+1}^n), & \text{if } \bar{u}_{c,i+1/2}^n < 0, \\ \mathbf{f}[\mathbf{U}^*(\mathbf{U}_i^n, \mathbf{U}_{i+1}^n)], & \text{else}, \end{cases}$$

$$\mathbf{F}_{\text{R}}(\mathbf{U}_{i-1}^n, \mathbf{U}_i^n) = \begin{cases} \mathbf{f}[\mathbf{U}^*(\mathbf{U}_{i-1}^n, \mathbf{U}_i^n)] + \mathbf{H}(\mathbf{U}_i^n, \mathbf{U}_{i+1}^n), & \text{if } \bar{u}_{c,i-1/2}^n > 0, \\ \mathbf{f}[\mathbf{U}^*(\mathbf{U}_{i-1}^n, \mathbf{U}_i^n)], & \text{else}, \end{cases}$$

$$\mathbf{H}(\mathbf{U}_i^n, \mathbf{U}_{i+1}^n) = \begin{bmatrix} -\bar{u}_{c,i+1/2}^n\cdot(\bar{\alpha}_{i+1}^n - \bar{\alpha}_i^n) \\ 0 \\ \bar{p}_{i+1}^n\bar{\alpha}_{i+1}^n - \bar{p}_i^n\bar{\alpha}_i^n \\ \bar{u}_{c,i+1/2}^n\cdot(\bar{p}_{i+1}^n\bar{\alpha}_{i+1}^n - \bar{p}_i^n\bar{\alpha}_i^n) \\ 0 \\ -(\bar{p}_{i+1}^n\bar{\alpha}_{i+1}^n - \bar{p}_i^n\bar{\alpha}_i^n) \\ -\bar{u}_{c,i+1/2}^n\cdot(\bar{p}_{i+1}^n\bar{\alpha}_{i+1}^n - \bar{p}_i^n\bar{\alpha}_i^n) \end{bmatrix}.$$

Here $\mathbf{U}_i^{n+1}$ is the unknown grid function, i is the spatial index and n is the time index. The key point of the numerical algorithm is the construction of the Riemann problem solution $\mathbf{U}^*(\mathbf{U}_i^n, \mathbf{U}_{i+1}^n)$ for the Baer-Nunziato system of equations. This solution has two distinct cases: the case where solid phase exists on both sides of the computational cell edge, and the case where the solid phase vanishes. The

solid contact velocity, $\bar{u}^n_{c,i+1/2}$, is obtained from the solution to the Riemann problem. If $|\bar{\alpha}^n_{i+1} - \bar{\alpha}^n_i|$ is small enough the defining system of equations can be decoupled into two Euler systems, which are solved using a common Godunov method [35]. The details of this numerical algorithm can be found elsewhere [21]. Note that solving Baer-Nunziato-type equations poses significant challenges, and the developing accurate and efficient numerical methods for solving these systems remains a current area of research [36 – 38].

3 Simulation Results

A uniform grid with a cell size of $\Delta x = 1$ mm is used to analyze the main features of the flow field in the process that could be responsible for the formation of pressure peaks on transducers D2 and D3. Figure 6 shows the record of transducer D1. The high-pressure chamber produces a one-meter-long pulse with a constant amplitude, followed by a rarefaction wave (see Figure 6a). This looks like a localized structure in Figure 6c. Around 5.5 ms, the first incident pulse interacts with the particle bed near the wall (see Figure 6b). The reflected pulse from the bed appears as a second localized structure in Figure 6b, and so on.

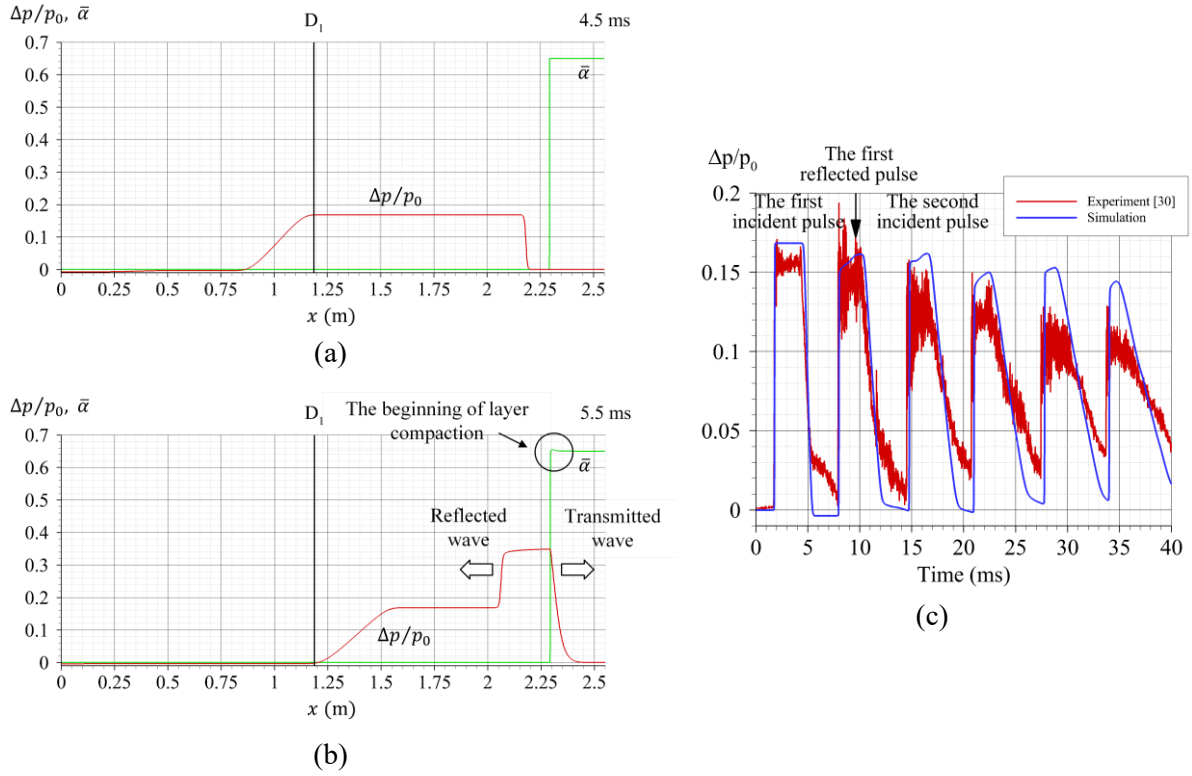

Figure 6: Generation of pulses on the D1 transducer.

Figures 7 and 8 show a comparison of experimental and calculated data for the pressure transducers D2 – D4. In Figure 7a, the blue line represents the gas pressure in the simulation, and the orange line represents the solid phase pressure. We can see that the waves in the particle phase are in the form of peaks on the smooth waves of the gaseous phase. For the second and the third "hills", the peaks are located on the falling part of the blue curve. As in [21], we compared the volume-averaged pressure $p_{mix} = \bar{\alpha}\bar{p} + \alpha p$ with the experimental pressure record (see Figure 7b). This p_{mix} mimics the operation of the pressure transducer in the experiment. The averaging procedure reduces the peak due to the solid phase pressure at the top of the first blue "hill" and makes the amplitudes of the peaks for the second and third hills much closer to the experimental values.

For the pressure transducer D3 the correlation between the simulated and experimental data can also be considered satisfactory (see Figure 8a). With the exception of a pronounced peak at approximately 10 ms and the splitting of the main peak, the simulation results describe the real-life phenomenon well. However, for transducer D4, a qualitative difference was obtained between

computed and experimental data (see Figure 8b). In experiments, the signal on D4 was almost damped compared to D2 and D3 (see the cyan line in Figure 8b). In simulations, this behavior is only valid for gas pressure (see the green line in Figure 8b), while waves in the solid phase produce peaks similar to those in D2 and D3. This means that, although the obtained results are reasonable in many aspects, some important features of the flow have been missed, and further study on modeling issues is needed.

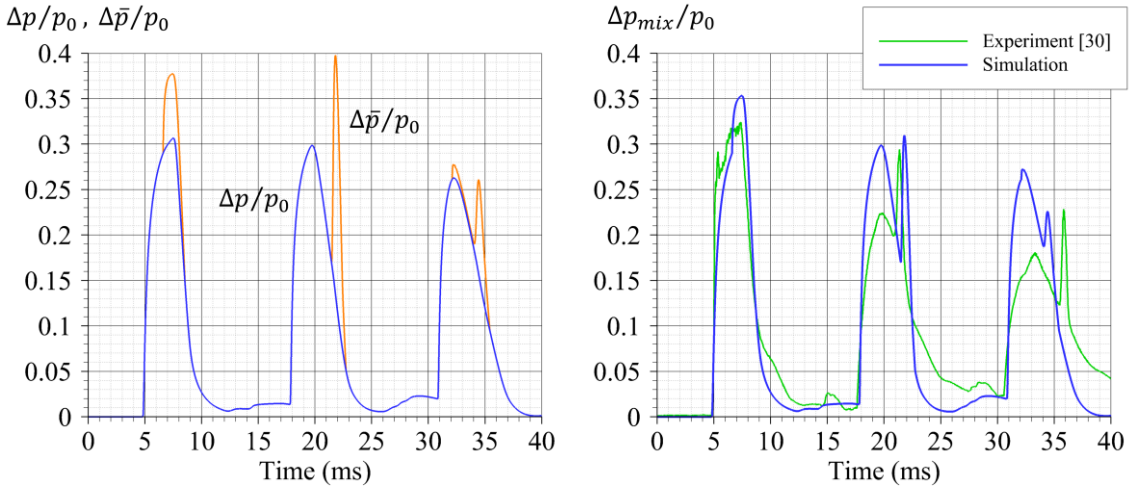

Figure 7: Comparison of experimental and calculated data for pressure transducer D2.

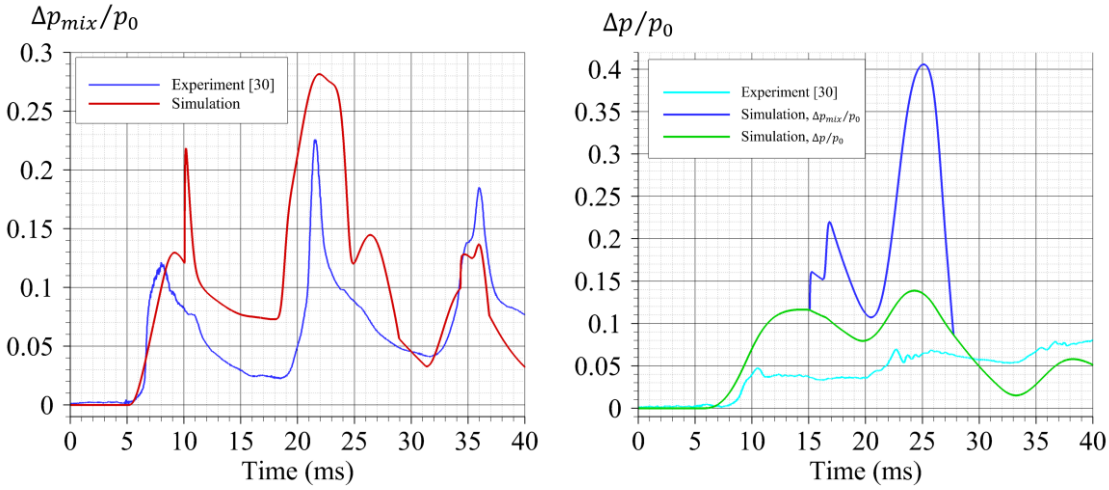

Figure 8: Comparison of experimental and calculated data for pressure transducers (a) D3 and (b) D4.

Let's analyze the mechanisms of peaks formation in transducers D2 – D4. Figure 9 shows wave dynamics inside the bed after the impact of the first pulse from gas. This pulse produces a compression wave in the gaseous phase propagating inside the bed. The key factor that determines the wave dynamics in the solid phase is the model for the potential energy of compaction (1), which has a "yes-no" switching form depending on the $\bar{\alpha}_{\text{crit}}$ parameter. Parameters chosen produce a compaction wave immediately after the shock wave impact, resulting in an additional orange peak associated with the intergranular stresses on the blue hill in Figure 7a. As you move deeper into the bed, the amplitude of the compaction wave decreases, even though the model uses a stiff pressure relaxation with no finite value for the compaction viscosity parameter μ_c. The peaks on D3 at 10 ms and on D4 at 15 ms are caused by this compaction wave.

The second pulse interacts with a bed that has already been compressed by the first pulse (see Figure 10). When a shock wave approaches the edge of the bed, a compaction wave begins to move in

the opposite direction from the bottom wall of the tube. These two waves combine to create a sharp peak on the D2 transducer at 22 ms. The spatial distributions of $\bar{\alpha}$ in Figures 9 and 10 also show a loosened region near the upper boundary of the bed that was formed as a result of the initial impact. In experimental studies [29, 30], a phenomenological model was proposed to explain pressure peaks with this region forming an important part of the process.

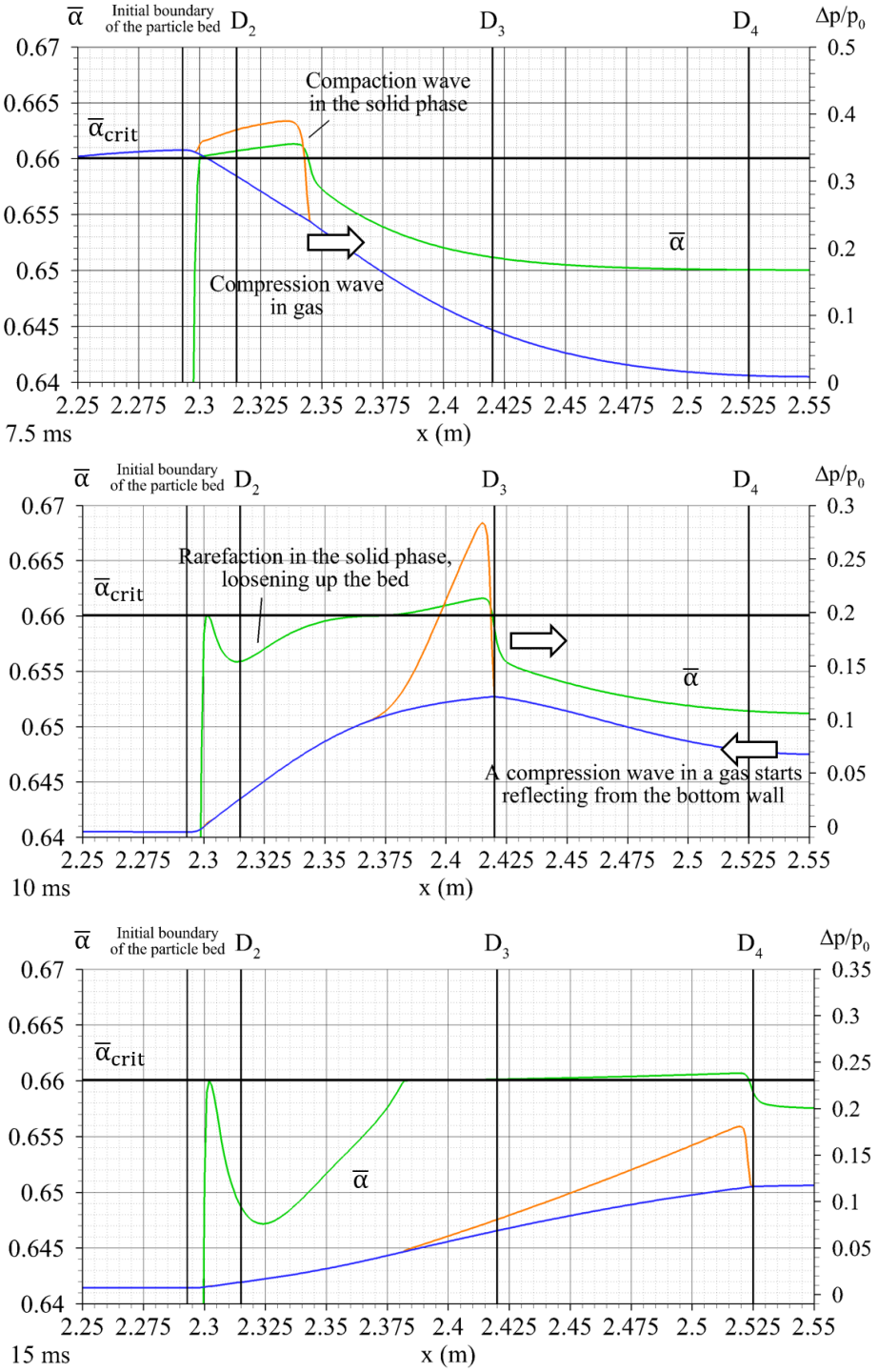

Figure 9: Waves propagation inside the bed after the impact of the first pulse. Green lines represent the predicted spatial distributions of $\bar{\alpha}$, blue lines represent $\Delta p/p_0$ for gas, and orange lines represent $\Delta\bar{p}/p_0$ for particles.

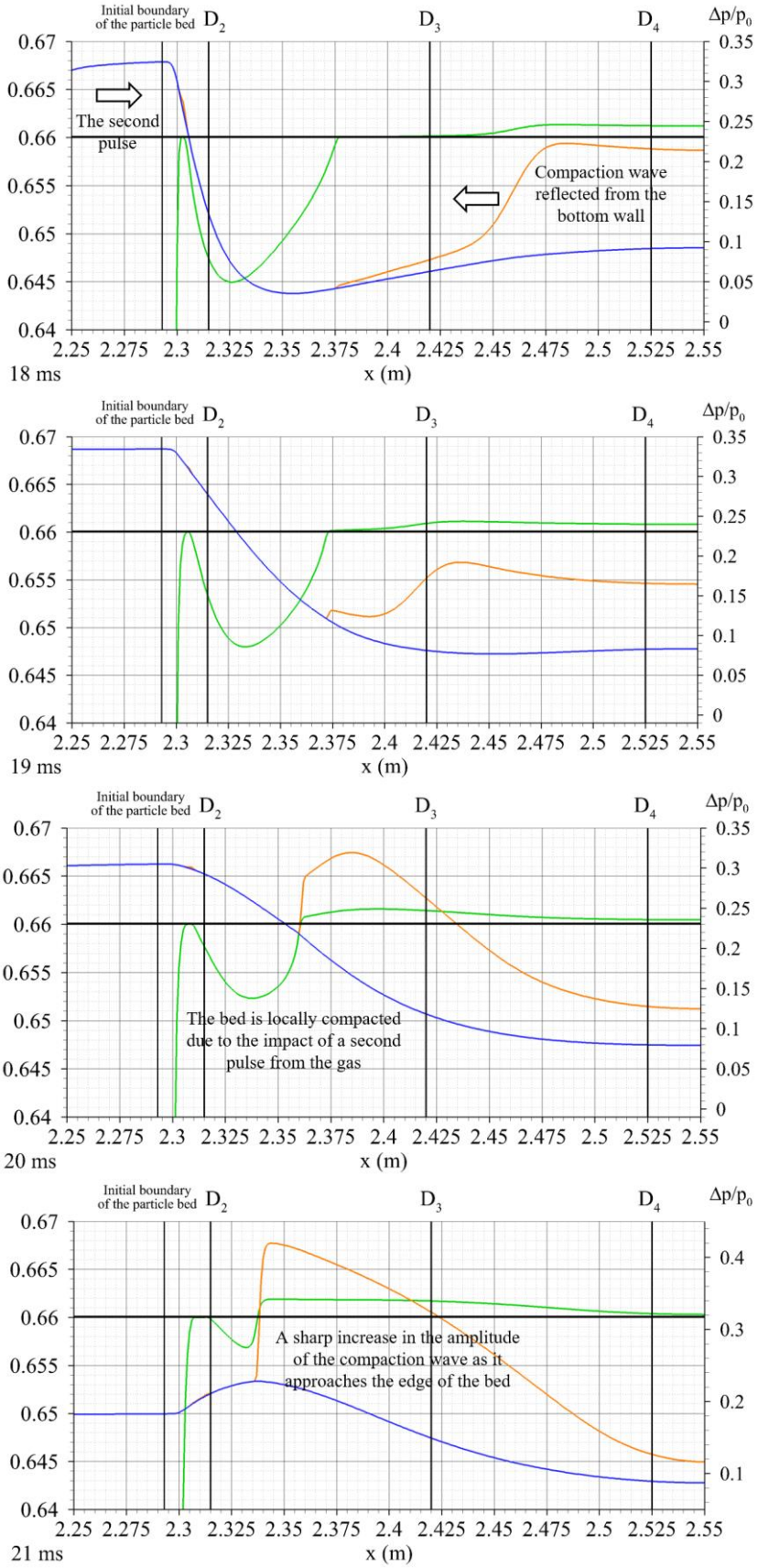

Figure 10: Waves propagation inside the bed after the impact of the second pulse. Green lines represent the predicted spatial distributions of $\bar{\alpha}$, blue lines represent $\Delta p/p_0$ for gas, and orange lines represent $\Delta \bar{p}/p_0$ for particles.

4 Conclusion and Future Work

The numerical simulation of the probing of a two-phase sand bed using multiple pulses of gas has been conducted. The mathematical model was based on the Baer-Nunziato equations, taking into account intergranular stresses within the solid phase. We have provided a possible explanation for the formation of pressure peaks on transducers within the bed, which has been observed recently in experiments [29, 30]. This effect was not observed in the experiments. One possible improvement to the model would be to consider the compaction viscosity within the solid phase, along with intergranular stresses, as was done in [33] for simulations of heterogeneous detonation. Another approach is to use a model for the potential energy of compaction that does not take into account the true density of the solid phase, but only its volume fraction, as was done in earlier studies [16, 39].

5 Acknowledgements

The author would like to express his gratitude to Prof. I. Gimaltdinov and Prof. A. Akhmetov for their valuable assistance in formulating the problem and providing clarifications regarding the experimental data.

References

[1] D. Wang, Q. Jing and Y. Cheng. Influence of dust layers in connecting pipes on explosion propagation characteristics of flake aluminum powder in cylindrical interconnected vessels. ACS Omega, 8:2197-2212, 2023.

[2] S. P. Medvedev, E. K. Anderzhanov, I. V. Guk, A. N. Ivantsov, A. I. Mikhaylin, M. V. Silnikov, V. S. Pomazov, A. M. Tereza and S. V. Khomik. Testing of explosion-proof coatings in cylindrical and conical shock tubes. Russ. J. Phys. Chem. B, 14:946-950, 2020.

[3] L. Zhang, H. Guan, Z. Feng, M. Sun and H. Jin. Modeling and simulation of a shock driving gas jet laden with dense extinguishant particles through a tube with a tail nozzle. Fire Tech., 59:3629-3666, 2023.

[4] B. S. Ermolaev and A. A. Sulimov. *Convective Burning and Low-Speed Detonation of Porous Energetic Materials*. Moscow: Torus Press. 2017 (in Russian).

[5] A. Chiapolino and R. Saurel. Numerical investigation of two-phase finger-like instabilities. Comp. & Fluids, 206:104585, 2020.

[6] M. Sun, J. Li, H. Zhang, R. Chi, B. Pang, W. Cao, J. Fan, J. Xu and J. Xiao. Effect of relative density and grain size on the internal flow field during the ballistic penetration of sand. Int. J. Impact Eng., 185:104859, 2024.

[7] J.-R. Li, J.-S. Zeng and K. Xue. Pressure evolution in shock-compacted granular media. Petr. Sci., 20:3736-3751, 2023.

[8] J. Capecelatro. Modeling high-speed gas-particle flows relevant to spacecraft landings. Int. J. Multiphase Flow, 150:104008, 2022.

[9] M. R. Baer and J. W. Nunziato. A two-phase mixture theory for the deflagration-to-detonation transition (DDT) in reactive granular materials. Int. J. Multiphase Flow, 12:861-889, 1986.

[10] Y. Sugiyama, T. Homae, T. Matsumura and K. Wakabayashi. Numerical study on the mitigation effect of glass particles lifting a partially confined space on a blast wave. Int. J. Multiphase Flow, 136:103546, 2021.

[11] D. Gidaspow. *Multiphase Flow and Fluidization*. Academic Press. 1994.

[12] T. A. Khmel' and A. V. Fedorov. Description of dynamic processes in two-phase colliding media with the use of molecular-kinetic approaches. Comb., Expl., Shock Waves, 50:196-207, 2014.

[13] R. Houim and E. Oran. A multiphase model for compressible granular–gaseous flows: Formulation and initial tests. J. Fluid Mech., 789:166-220, 2016.

[14] K. Shimura and A. Matsuo. Two-dimensional CFD-DEM simulation of vertical shock wave-induced dust lifting processes. Shock Waves, 28:1285-1297, 2018.

[15] R. I. Nigmatulin. *Dynamics of Multiphase Media*. Volume 1. First edition. CRC Press. 1990.

[16] A. G. Kutushev and D. A. Rudakov. Numerical study of the action of a shock wave on an obstacle screened by a layer of porous powder material. J. Appl. Mech. Tech. Phys., 34:618-624, 1993.

[17] A. A. Gubaidullin, A. Britan and D. N. Dudko. Air shock wave interaction with an obstacle

covered by porous material. Shock Waves, 13:41-48, 2003.
[18] M. Y. Nemtsev, I. S. Menshov and I. V. Semenov. Numerical simulation of dynamic processes in a medium of fine-grained solid particles. Math. Mod. Comp. Sim., 15:210-226, 2023.
[19] P. S. Utkin. Mathematical modeling of the interaction of a shock wave with a dense cloud of particles within the framework of the two-fluid approach. Russ. J. Phys. Chem. B, 11:963-973, 2017.
[20] P. S. Utkin. Numerical simulation of shock wave – dense particles cloud interaction using Godunov solver for Baer-Nunziato equations. Int. J. Num. Meth. Heat & Fluid Flow, 29:3225-3241, 2019.
[21] Ya. E. Poroshyna and P. S. Utkin. Numerical simulation of a normally incident shock wave – dense particles layer interaction using the Godunov solver for the Baer-Nunziato equations. Int. J. Multiphase Flow, 142:103718, 2021.
[22] X. Rogue, G. Rodriguez, J. F. Haas and R. Saurel. Experimental and numerical investigation of the shock-induced fluidization of a particle bed. Shock Waves, 8:29-45, 1998.
[23] A. Panchal, S.H. Bryngelson and S. Menon. A seven-equation diffused interface method for resolved multiphase flow. J. Comp. Phys., 475:111870, 2023.
[24] M. Petrella, R. Abgrall and S. Mishra. On the discrete equation model for compressible multiphase fluid flow. J. Comp. Phys., 478:111974, 2023.
[25] B. E. Gelfand, S. P. Medvedev, A. A. Borisov, A. N. Polenov, S. M. Frolov and S. A. Tsyganov. Shock loading of stratified dusty systems. Arch. Combust, 9:153-165, 1989.
[26] D. W. Schwendeman, C. W. Wahle and A. K. Kapila. The Riemann problem and a high-resolution Godunov method for a model of compressible two-phase flow. J. Comp. Phys., 212: 490-526, 2006.
[27] P. S. Utkin and P. A. Chuprov. Numerical simulation of shock wave propagation over a dense particle layer using the Baer-Nunziato model. Phys. Fluids, 35:113313, 2023.
[28] B. C. Fan, Z. H. Chen, X. H. Jiang and H. Z. Li. Interaction of a shock wave with a loose dusty bulk layer. Shock Waves, 16:179-187, 2007.
[29] A. T. Akhmetov, I. K. Gimaltdinov, M. A. Azamatov, A. F. Mukhametzyanov and D. R. Bogdanov. Sounding of water-gas-saturated bulk media by rereflected waves immediately after the impact of a shock wave. Tech. Phys. Lett., 48: 97-102, 2022.
[30] A. T. Akhmetov, I. K. Gimaltdinov and A. F. Mukhametzyanov. Revealing the conditions for the formation of pressure peaks in a probing pulse. Proc. Int. Conf. Mathematical Physics, Mechanics and Applications, Sterlitamak, Russia, 21 – 24 June 2023, 34-39 (in Russian).
[31] J. B. Bdzil, R. Menikoff, S. F. Son, A. K. Kapila and D. S. Stewart. Two-phase modeling of deflagration to-detonation transition in granular materials: A critical examination of modeling issues. Phys. Fluids, 11:378-402, 1999.
[32] A. K. Kapila, R. Menikoff, J. B. Bdzil, S. F. Son and D. S. Stewart. Two-phase modeling of deflagration to-detonation transition in granular materials: reduced equations. Phys. Fluids, 13:3002-3024, 2001.
[33] D. W. Schwendeman, C. W. Wahle and A. K. Kapila. A study of detonation evolution and structure for a model of compressible two-phase reactive flow. CTM, 12:159-204, 2008.
[34] R. Saurel, N. Favrie, F. Petitpas, M.-H. Lallemand and S. L. Gavrilyuk. Modelling dynamic and irreversible powder compaction. J. Fluid Mech., 664:348-396, 2010.
[35] E. F. Toro. *Riemann Solvers and Numerical Methods for Fluid Dynamics.* Third Edition. Springer, 2009.
[36] A. Serezhkin and I. Menshov. On solving the Riemann problem for non-conservative hyperbolic systems of partially differential equations. Comp. & Fluids, 210:104675, 2020.
[37] C. Zhang, L. Wang, Z. Shen, Z. Li and I. Menshov. A reduced model for compressible viscous heat-conducting multicomponent flows. Comp. & Fluids, 236:105311, 2022.
[38] R. R. Polekhina, B. A. Korneev and E. B. Savenkov. Numerical study of hyperbolic models. J. Comp. Appl. Math., 423:114925, 2023.
[39] P. S. Gough and F. J. Zwarts. Modeling heterogeneous two-phase reacting flows. AIAA J., 17:17-25, 1979.